IEEE Access
Multidisciplinary | Rapid Review | Open Access Journal

Received February 19, 2019, accepted April 18, 2019, date of publication April 22, 2019, date of current version May 3, 2019.

Digital Object Identifier 10.1109/ACCESS.2019.2912564

Detecting All Possible Ionospheric Precursors by Kernel-Based Two-Dimensional Principal Component Analysis

JYH-WOEI LIN, JUING-SHIAN CHIOU, AND CHUN-TANG CHAO
Department of Electrical Engineering, Southern Taiwan University of Science and Technology, Tainan 71005, Taiwan

Correspondence author: Juing-Shian Chiou (jschiou@stust.edu.tw)

This work was supported by the Ministry of Science and Technology, Taiwan, under Grant MOST 106-2221-E-218-001-MY2.

ABSTRACT Kernel-based two-dimensional principal component analysis (K2DPCA), a nonlinear method, was performed to examine ionospheric 2-D total electron content (TEC) variations obtained from the NASA Global Differential GPS (GDGPS) network, which consisted of low spatial resolution ionospheric TEC data, to detect TEC precursors prior to the China Ludian earthquake at 08:30:13 UT on 03 August 2014 ($M = 6.1$). Simultaneously, two-dimensional principal component analysis (2DPCA), a linear method, was performed to examine data related to the same earthquake for comparison purposes. The results have shown that two TEC precursors were observed three days prior to this earthquake. The characteristics of all principal eigenvalues were considered to determine the TEC precursors of the earthquake in this paper. This paper aimed to differentiate the previous studies of Lin about 2DPCA using only the characteristic of the first principal eigenvalue to determine the TEC precursors of the earthquake. However, some other TEC precursors could be lost in processes that do not analyze the characteristics of other principal eigenvalues. Therefore, this research can be considered as a full analysis that examined the detailed surrounding TEC precursors of the earthquake and could be treated as a new study scope with 2DPCA and K2DPCA. The TEC precursor during 06:15 to 06:20 (UT) on 01 August 2014 localized near the epicenter was more intense compared with the characteristic of the first largest principal eigenvalue. However, another localized TEC precursor, which occurred from 06:15 to 06:20 (UT) on 01 August 2014 at a site west of the epicenter, was found to be more intense. The more plausible reason for the two TEC precursors could be the density variances caused by radon-gas release due to the fine crack stress transfer from the rocks according to Coulomb stress transfer theory as applied to a far TEC precursor. The durations of both TEC precursors were at least 5 min. This research could be treated as a full and detailed examination of surrounding TEC precursors. K2DPCA was better at identifying the TEC precursors.

INDEX TERMS Kernel-based two-dimensional principal component analysis (K2DPCA), 2D total electron content (TEC), TEC precursors, NASA global differential GPS (GDGPS) network, two-dimensional principal component analysis (2DPCA), China Ludian earthquake, Radon-gas release, Coulomb stress transfer theory.

I. INTRODUCTION

A. IONOSPHERIC ANOMALIES DUE TO EARTHQUAKES

The ionosphere is the ionized part of Earth's upper atmosphere, extending from a height of 60 km to 1,000 km and ionized by solar radiation. It includes the thermosphere and parts of the mesosphere and exosphere. It has an important role in the generation of atmospheric electricity and forms the inner edge of the magnetosphere. It influences radio propagation to distant places on the Earth [36]. Ionospheric total electron content (TEC) is an important descriptive quantity for the ionosphere, which is defined as the total number of electrons integrated between two points. A TEC unit is TECu (10^{16}electrons/m^2) [16]. Ionospheric TEC precursors of large earthquakes have been widely researched both as precursors and after effects ([43], [45], [62], [31], [19], [12], [20], [46], [38], [49], [52], [1], [24], [40]). Ionospheric TEC precursors of earthquakes are generally of two types: physical

The associate editor coordinating the review of this manuscript and approving it for publication was Bora Onat.

and chemical precursors. The physical precursor includes water level, temperature, and conductivity. The chemical precursor includes chemical components and gases, e.g., radon gas of groundwater and soils in a fault zone, which is proven to play an important role in earthquake short-term prediction [11]. Reference [43] presented an extensive list of possible causes, including radon-gas release, which cause lower atmospheric electric fields that travel up into the ionosphere along the geomagnetic lines. Meanwhile, [8] proposed the P-type semiconductor effect as the cause of lower atmosphere electric fields. The P-type semiconductor effect is caused by charge separation that occurs in metamorphic, near-cracked, and igneous rocks among the electrons in the stressed range of rocks and small positive holes (i.e., p-holes) that appear away from the stressed regions. Once positive holes are generated, some phenomena occur as current propagates through the rocks, resulting in electromagnetic emissions. If the true cause can be known, as previously stated, then development of earthquake prediction would be good. The exact causes of TEC precursors of earthquakes are not known. However, many possibilities are present, including gravity waves generated by the solid earth and sea and lower atmospheric electric fields resulting from the earthquake-generation processes that can be transmitted into the ionosphere along geomagnetic lines [44]. Regardless of the specific causes of the earthquake-precursor TEC anomalies, their earthquake association has been statistically established by deviations using the TEC median values after eliminating other possible causes of the TEC disturbance, such as solar flare and geomagnetic storm activity. A solar flare is a sudden flash of increased brightness on the sun observed near its surface close to a sun spot. Sun spots are phenomena on the photosphere of sun, which appear as spots and are darker than the surrounding regions. They are regions of reduced surface temperatures, which are caused by concentrations of magnetic field flux. A geomagnetic storm is a severe disturbance of the magnetosphere of the earth caused by strong solar winds, and it compresses the magnetosphere. The solar wind is a stream of charged particles released from the upper atmosphere of the sun. This plasma consists of mostly electrons, protons, and alpha particles, which are embedded within the solar-wind plasma in the interplanetary magnetic field ([55], [48]).

B. RELATED STUDIES OF TEC PRECURSORS

In this section, the analysis results of a few important and valuable existing studies on TEC precursors are described and then summarized to introduce the research purpose of this study. Reference [31] observed the variations in TEC associated with 35 $M \geq 6.0$ earthquakes that occurred in China during the 10year period from May 1, 1998 to April 30, 2008. The statistical results indicated that TEC near the epicenter often pronouncedly decreased in three to five days before the 17 $M \geq 6.3$ earthquakes. The TEC data were obtained from six microsatellites of FORMOSAT3/COSMIC. The TEC data were further used to observe the TEC anomalies during an $M = 8.0$ earthquake near Wenchuan, China, on May 12, 2008. TEC above the forthcoming epicenter was found to anomalously decrease in the afternoon period in the fourth to sixth days and in late-evening period on the third day before the earthquake but was enhanced in the afternoon in the third day before the earthquake. Reference [19] adopted a soft computing technique to identify TEC anomalies related to earthquakes with low latitude TEC data using the peak-detection technique and dynamic time-warping algorithm for pattern reorganization. This is the first step in utilizing this approach for identification of an impending earthquake. They identified a signature of strong earthquakes with $M > 6$ when the observing station is within the earthquake-generation zone. However, this method suffers from the limitation in that it cannot resolve fine structures, e.g., changes in times, because of the enormous increase in the size of the matrix required to compute such changes. Reference [12] statistically investigated the TEC anomalies before large earthquakes around the regions in Japan from 1998 to 2012 using the superposed epoch analysis (SEA) and Molchan's error diagram (MED) analysis. These methods were used to investigate the correlation and predictability in a statistical manner. The SEA results have indicated positive anomaly from one to five days before a large earthquake ($M \geq 6.0$; depth ≤ 40 km). However, the results of the MED analysis indicated some gain compared with the random estimation called Poisson model. Reference [20] used the pattern-reorganization technique (a pattern-matching technique) to monitor TEC variations during and prior to earthquakes. In his experiment, an earthquake, i.e., the TEC precursor two days before the Bhutan earthquake on September 21, 2009, was considered for TEC data analysis, which was based on the TEC data collected from the GPS at Gauhati (26° 10' N, 91° 45' E) and National Oceanic and Atmospheric Administration satellite data. Reference [21] analyzed the TEC variations and atmospheric refractivity prior to the Iran earthquake that occurred on April 16, 2013 (28.10° N, 62.05° E) obtained from two GPS-based TEC receivers in Surat (21.16° N, 72.78° E) and Lucknow (26.91° N, 80.95° E). The results of the atmospheric refractivity profile from the radiosonde observation stations (in Shiraz, Iran and Delhi, India) around the fault line were presented. The atmospheric refractivity was modified six to eight days before the earthquakes in Shiraz, Iran and Delhi, India. To search the precursor signatures of an earthquake, TEC variations and refractivity are important parameters [33]. The ionospheric TEC started approximately 40 min before the 2011 Tohoku-Oki. Reference [13] examined the TEC enhancement that occurred ~40 min before the 2011 Tohoku-oki (Mw9.0) earthquake in Japan with Global Navigation Satellite Systems receivers. Their reality has been repeatedly questioned mainly owing to the ambiguity in deriving the reference TEC curves from which the anomalies were defined.

Reference [46] analyzed the GPS-TEC data received at Agra station, India (27.2° N, 78° E), and the diurnal variations in the global ionospheric map (GIM) TEC data near the

epicenter of this earthquake ($M = 7.8$) in a Pakistan region in the month of April, 2013 were examined. A statistical technique that analyzed the data and identified the significant precursors using a 3σ criterion was employed. These TEC precursors were detected five to seven days prior to this earthquake. Reference [50] used five models of ionospheric anomalies due to earthquakes to demonstrate significant TEC anomalies prior to large earthquakes in Japan. The GIM-TEC method has been used to identify combined anomalies due to seismic activities. After finding the combined anomalies, they were filtered using the GIM-TEC star method to obtain the specific anomaly related to earthquakes. The global model of a TEC anomaly uses only the interpolated TEC data for local interpolation. The Kriging method localizes the area of anomaly related to the position of the epicenter area. Therefore, the ionosphere precursor covers the whole territory of Japan ($30° - 45°$ LU, $125° - 155°$ BT). Using neural network, the epicenter area was estimated ($\approx 2.5° \times 5°$). For the $M = 6.1$ earthquake that occurred on August 10, 2009, the changes showed that the ionospheric precursor anomalies appeared five days before the earthquake at precisely 12.00 UT on August 5, 2009 from the results of the GIM-TEC star models with Kriging interpolation. For the $M = 6.6$ earthquake that occurred on July 16, 2007, the ionospheric precursors appeared five days before the earthquake at precisely 12.00 UT on July 11, 2007 from the results of the GIM-TEC star models with Kriging interpolation. For the $M = 6.3$ earthquake that occurred on December 20, 2008, the ionospheric precursors appeared three days before the earthquake at precisely 03.00 UT on December 17, 2008 from the results of the GIM-TEC star models with Kriging interpolation. For the $M = 6.9$ earthquake that occurred on June 13, 2008, the ionospheric precursors appeared two days before the earthquake at precisely 21.00 UT on June 11, 2008 from the results of the GIM-TEC star models with Kriging interpolation. For the $M = 6.4$ earthquake that occurred on June 5, 2009, the ionospheric precursors appeared three days before the earthquake at precisely 19.00 UT on June 2, 2009 from the results of the GIM-TEC star models with Kriging interpolation. These previous TEC anomalies were always located near the epicenter area. The success of the neural network in estimating the epicenter area presented a new stage of development of an earthquake-prediction method.

Reference [57] described their geological observation using continuous MODIS/Terra satellite remote-sensing thermal infrared data of this earthquake region in Ludian, Yunnan, from June to August 2014. The active fault before and after the earthquake was analyzed. The latent heat-flux changes were studied. They proposed that the anomalous phenomenon due to temperature increase in the active fault could be a short-term precursor of the earthquake. The release of radon gas in the groundwater caused by heat-flux changes could be a possible precursor.

Reference [38] measured the TEC variations prior to two large earthquakes in Nepal ($M = 7.8$) and Chile ($M = 8.3$) in 2015 obtained from the Global Navigation Satellite System (GNSS) network (International GNSS Service network). Statistical and spectral analyses were applied to show the abnormal TEC variations, which appeared from few days up to few hours before the events that lasted up to 8 h. The intensified TEC variations were identified as a type of wave-like oscillations with periods of 20 and 2–5 min. These oscillations could be linked to impending earthquakes. An unusual modification of the equatorial ionospheric anomaly five days before these earthquakes was also confirmed. Spectral analysis of the TEC satellite measurements proved the difference between the seismically induced ionospheric waves and those with different origins, such as geomagnetic storms. However, the analysis method was still used to measure the TEC variations. They did not use a mathematical tool. Reference [17] examined the TEC variants for April 15, 2016, for the Kumamoto earthquake (Mw 7.3) that occurred in Japan using GNSS receivers. The TEC anomaly was detected several tens of minutes before the 2016 Kumamoto earthquake near its epicenter. Reference [49] measured the TEC variation in the ionosphere using the GNSS data. The TEC data were induced by earthquakes in the Himalayan region. The results were analyzed together with the other inducing factors, e.g., geomagnetic storm and solar flares [5], which affected TEC, to limit the causative factor. Their results indicated TEC anomalies in the ionosphere as evidence few days prior to the seismic event. The TEC variations increased as the epicenter distances decreased relative to the 2015 Nepal earthquake ($M = 7.8$). These TEC variations increased by 15–20 TECu recorded at stations separated apart by 60 km. They also provided a method for epicenter detection based on the TEC concentration, which increased closer to the epicenter. TEC variations were observed during a period of zero to eight days prior to four earthquakes: the April 1, 2015 Pipalkoti earthquake (4.9 Mw), April 25, 2015 Nepal earthquake (7.8 Mw), April 26, 2015 Nepal earthquake (6.7 Mw), and May 12, 2015 (7.3 Mw) Nepal earthquake. Reference [52] monitored the TEC changes in TECu. GPS satellites have begun to be used to monitor ionospheric TEC anomalies before earthquakes since they started to be used as sensors around the world. For three fault types (normal, thrust, and strike-slip faults) of 28 earthquakes with magnitudes of greater than 7.0, the percentage changes in the TEC anomalies before these earthquakes were investigated. The ionospheric TEC anomalies before the earthquake were calculated according to a 15-day running-median statistical analysis method [30]. The TEC anomalies were determined during the quiet days before an earthquake by comparing the ionospheric anomalies that occurred before an earthquake after the determination of the quiet days using the indexes of the space weather conditions e.g., solar wind [5], [35]. The results demonstrated the relationship between the fault type and earthquake precursor percentage changes, i.e., 47.6% TECu for regions with normal faults, 50.4% TECu for regions with thrust faults, and 44.2% TECu for regions with strike-slip faults were determined.

Reference [54] analyzed the TEC data before the earthquake struck using the Sumatran GPS Array (SuGAR) from September 2007 until September 2012 and observed that 12 earthquakes occurred with magnitude > 6.0 over Sumatra, Indonesia. using the correlation technique. The correlation technique with anomaly values were used to identify ionospheric variation related with earthquake preparation. In result, ten of them were preceded by the TEC anomaly 1 to 24 days before the earthquakes struck. Reference [1] surveyed the variations in TEC,, aerosol optical depth (AOD), and skin temperature (SKT) using an absolute scalar magnetometer, a vector-field magnetometer, and an electric-field instrument on board Swarm satellites. GPS measurements, MODIS-Aqua satellite, and the European Center for Medium-Range TEC anomalies occurred on the eight and one to five days before the earthquakes. Some TEC anomalies were observed within one day after the earthquakes due to acoustic resonance of the aftershocks. Reference [10] investigated the TEC variation related to the February 5, 2016 (UTC) Tainan earthquake with ML $= 6.6$. The TEC data were calculated using the phase delays of the signals observed from the densely arranged ground-based stations in Taiwan for GNSS. The anomalies were observed within 1 h before this earthquake. Reference [14] conducted three–dimensional tomography of ionospheric electron density anomalies immediately before the 2015 Illapel Mw $= 8.3$ earthquake, Central Chile, using five GPS and five GLONASS satellites and applied continuity constraints to regularize the linear least squares inversion. The reconstructed anomalies are composed of positive and negative regions at altitudes of $\sim$200 km and $\sim$400 km, respectively, distributed roughly along the geomagnetic field.

The results of the previous studies are summarized as follows: **(1)**The analysis methods to detect TEC precursors were based on the observation and measurement of TEC variants that were still commonly used at the time. **(2)** That the increase and decrease in TEC were earthquake precursors was still an argument. **(3)** Expensive TEC receiving network systems, e.g., GNSS [17] were used, which is more expensive than GDGPS for the process of receiving TEC data. Moreover, a lot of researchers need to process TEC data. **(4)** The mathematical algorithms, e.g., dynamic time-warping algorithm [19], were only used to distinguish earthquake-related TEC anomalies from other unknown TEC anomalies. **(5)**The quality of the analysis, researching observing TEC variants as TEC precursors, was always affected by space weather conditions. Solar wind also affects the TEC variation. A special factor is the geomagnetic storm caused by solar flares. The TEC anomalies related to earthquakes were observed to be influenced by geomagnetic quiet days, although in some of these studies, mathematical tools were used to investigate the TEC variations. (6) Their results demonstrated that the TEC precursors were mostly located over the epicenter. Moreover, TEC data processing was complicated, which could require considerable examination time to sufficiently determine the earthquake TEC precursors instead of short-term prediction, e.g., within 1 h before an earthquake [10]. Therefore, the aim of this study is to identify the ionospheric TEC precursors, which are generally detectable, using a type of mathematical tool without the disadvantage of the previous methods so that the research method and the data acquisition should be not as expensive as possible and the data processing is not complicated thereby making it a better survey method dealing with TEC precursors. Recent studies have shown that TEC precursors could be represented by first principal eigenvalues with the largest magnitude via Two-dimensional principal component analysis (2DPCA) [26]. The behavior of first principal eigenvalues is not influenced by non-earthquake-associated TEC variants, which are a result of the effects of space weather conditions, particularly according to Figure 5b in the study by [25], which was conducted during a geomagnetic storm and involved first principal eigenvalues of small magnitude. The results confirmed that Principal Component Analysis (PCA) could improve the quality of TEC precursor detection, thus overcoming the disadvantages of earlier methods. Therefore, from the studies by [25], it is evident that the principal eigenvalues could serve as indicators of TEC precursors. However, other possible TEC precursors might be lost in processes that do not consider the characteristics of other principal eigenvalues. The PCA and 2DPCA are alternative pure mathematical methods for measuring TEC anomalies compared with the previous methods. These methods rely on exploiting the signal delay between the GPS satellites and ground receiver stations without directly observing ionospheric TEC. The long-term period variance in ionospheric TEC does not affect the outcome of the PCA and 2DPCA, and the potential influence of the geomagnetic storm are eliminated [25] because the TEC enhancements caused by geomagnetic storms and the magnitude of their corresponding principal eigenvalues are small. The result of the study by [25] was used to prove that no influence was exerted by the geomagnetic storm on the TEC precursor detection of earthquakes. Though, the PCA experiment was able to detect the TEC precursors [25], PCA might not be as immaculately useful as2DPCA in the detection of TEC anomalies when applied to two-dimensional TEC data [26]. 2DPCA is determined to reduce the high-dimensional 2D data into the low-dimensional matrix of principal eigenvalue to facilitate fast computing without distortion. However, the studies of [26] only identified the characteristic of the first principal eigenvalue to examine the ionospheric TEC precursors prior to these earthquakes, which was considered as a detailed TEC anomaly analysis. Such analysis could cause loss of information due to other TEC precursors, especially low ionospheric spatial resolution TEC data from the GDGPS Network. Reference [26] examined 2D TEC data from FORMOSAT-3 satellite system during the period from 7 to 12 May, 2008, which was five days before China Wenchuan earthquake (Mw $= 7.9$) on 12 May 2008. A TEC precursor represented with a larger first principal eigenvalue was detectable during the period from 02:00–04:00 UT on 9 May 2008 over the epicentre for the duration of

approximately 2 hours. Reference [27] identified the characteristic of the first principal eigenvalues of 2DPCA to detect TEC anomalies of 2D TEC data from the NASA Global Differential GPS system (GDGPS) associated with three Japan Miyako earthquakes with close epicentres. The first Miyako earthquake was the Mw = 6.7 Miyako earthquake that occurred in Japan on 16 February 2015. From 04:40 to 04:50 (UT) on 15, February, 2015, a TEC precursor was detected over the epicentre related to this Miyako earthquake with a duration of at least 10 minutes. The second Miyako earthquake with Mw = 6.3 occurred on 20 February 2015. Second TEC precursor related to this Miyako earthquake was recorded over the epicentre between 10:20 and 10:30 (UT) on 19 February with a duration of at least 10 minutes. The third Miyako earthquake with Mw = 6.1 occurred on 21 February 2015. A TEC precursor related to this earthquake was recorded over the epicentre between 04:15 and 04:25 (UT) on 20 February with a duration of at least 10 minutes.

However 2DPCA is a linear method [58], [22]. The behavior of ionospheric plasma is nonlinear [48], [55], and a type of 2DPCA called Kernel-Based Two-dimensional principal component analysis (K2DPCA), by which such nonlinear behavior is analyzed, is suitable because K2DPCA is a nonlinear method [22]. K2DPCA and Kernel Principal Component Analysis (KPCA) are common and have been successfully applied for face recognition [25], [6], [3], [18].

Reference [6] proposed a novel approach based on 2DPCA and KPCA, wherein, 2DPCA was first performed to project the faces onto the feature pace and then KPCA based on Euclidean distance was performed an experiment on ORL face database, Yale face database, and FERET face database. Results show that a high recognition rate of 100% and better performance than state-of-the-art approaches and promising applications could be achieved.

Reference [3] suggested a face recognition analysis based on Hybrid Gaborlet and Kernel Fisher Analysis (KFA). Flustered SVD (Fsvd) was used to derive an illumination invariant image. Discrete wavelet transform (DWT) could disintegrate the image into wavelet sub-bands. Hybrid Gaborlet was used extricate facial features. KPCA was used to reduce the dimensions of the image. Non-linear mapping and Fisher analysis were performed by KFA. The excellent recognition had good precision using Dr. Libor Spacek and Caltech segmented databases

Reference [18] proposed a patch-based principal component analysis (PCA) method to deal with face recognition. The face images were divided into patches to column vectors into a new image matrix by replacing the application with 2DPCA. Extensive experiments on the ORL and FERET face database were reported to have better accuracies than PCA and 2DPCA.

In a study on 2DPCA, [51] improved the image recognition rate for the extraction of image features through combining 2DPCA with wavelet theory in by standard ORL face recognition database. A simulation experiment was performed to obtain better accuracy for this proposed algorithm. Analysis results of K2DPCA should be better than those of 2DPCA for identifying TEC precursors. Moreover, thus far, there has been no relevant literature that reports on TEC precursors using K2DPCA. Reference [29] proposed a kernel-fusion based dimensionality combined reduction framework using the concept of kernel called Kernel Product (KP), Kernel Sum (KS) and Kernel Canonical Correlation Analysis (KCCA) to generate meaningful seismic representations from a non-linear one-dimensional seismic data set based on 2023 events in Israel and Jordan. PCA was used as a tool to reduce the dimension of the data while preserving most of the variance.

However the data will lose some information, particularly for 2D data, which will result in data-processing errors. Moreover, for to research face recognition, dividing the images into subimages was necessary, and then a large image-processing error would be caused [4]. Finally, summarizing the previous studies, at least two algorithms must be applied to result in complicated data processing.

The objective of this study is to identify the characteristics of all principal eigenvalues using K2DPCA to detect all possible TEC precursors comprehensively prior to the China Ludian earthquake (27.245° N, 103.427° E) at 08:30:13 UT on August 3, 2014 ($M = 6.1$), within a depth of 10.0 km (U.S. Geological Survey) from the surface and without the influence of non-earthquake TEC anomalies. Simultaneously, the results of K2DPCA will be compared with the results of 2DPCA to identify the TEC precursors. K2DPCA is also a mathematical tool that is more objective in comparison to the results of previous studies by other researchers. The possible causes of the discovered anomaly are discussed in detail. Moreover, only one algorithm is necessary, and the complicated data processing is avoided, thereby reducing the cost of data processing.

When detecting TEC precursors, the analysis was affected by non-earthquake TEC anomalies in previous studies. However, the data processing of 2DPCA is not complicated and the computing time is short, such that large data processing errors will not be caused, particularly for TEC data with low ionospheric TEC spatial resolution [26], [27]. Thus, more detailed TEC precursors can be detected under the condition of low ionospheric TEC spatial resolution of the TEC data, where other TEC precursors could not be detected from the analysis results of Lin's previous studies (2014 and 2016). This study will mitigate the disadvantages of Lin's previous studies (Lin, 2014 and 2016) using K2DPCA. Therefore, this study has new findings, and differs from Lin's previous studies.

II. TEC DATA SOURCE

The 2D TEC data of the F layer in the ionosphere are obtained from the NASA Global Differential GPS (GDGPS). The F layer, known as the Appleton–Barnett layer, extends from about 150 km to more than 500 km above the surface of the Earth. It is the layer with the highest electron density, and

does not disappear at night time, meaning it exists all day long [36]. The global TEC maps in the current study are obtained using the TEC data from approximately 100 real-time GDGPS tracking sites, which are augmented with additional sites that are available on a 5-min basis. The integrated electron-density data in each receiver-GPS satellite link is processed using a Kalman filter [59] in a sun-fixed frame to produce the GIMs. The core of the GDGPS network is the NASA GPS Network (GGN), a JPL-owned and operated network of roughly 70 geodetic-quality dual-frequency receivers that are globally distributed. Additional real-time sites are provided by various U.S. and international partner organizations. The result is the largest real-time GPS tracking network in the world with more than 100 global sites. All these sites stream their GPS measurements at 1 Hz to the GDGPS Operation Centers (GOCs) where they are processed and analyzed in real time. The GDGPS network is designed to be highly redundant to provide a unique measure of reliability for many critical applications that depend on it, such as real-time GPS integrity monitoring and precise differential corrections. On average, the network is 25-fold redundant (meaning that at any given time, each GPS satellite is observed by 25 ground sites, on average) and is minimally 10-fold redundant. Various communications channels are used for the raw measurements from the tracking sites to the GOCs, including the Internet, dedicated landlines, and satellite links. When the Internet is used, the data are sent in parallel to multiple GOCs to ensure redundancy of the Internet channels. All GOCs are interconnected to a Frame Relay or T1 line. The GDGPS boasts of four national timing laboratories among its contributing network partners. In particular, the United States Naval Observatory (USNO) provides two monitoring sites operated by its Master Clock, which allow GDGPS to provide its global users the most accurate real-time realization of USNO UTC. In addition, many GDGPS sites are driven using atomic-frequency standards, which provide robust data-quality schemes. Because we own and operate a vast majority of the tracking sites, we can configure the receivers to extract all GPS data, including TEC data, all L1 and L2 phases and pseudorange measurements, navigation messages, signal-to-noise values, and other civilian GPS data. It typically takes approximately 1 s for the GPS tracking data from most of the monitoring sites to reach the GOCs and a few more seconds for processing and quality control. The final products, such as precise corrections of the GPS broadcast ephemeris, are transferred within 5 s from the GPS data collection points to the remote sites. To ensure the integrity of the GDGPS products, the data from the GGN core of the network are authenticated. Consequently, the system is immune to data spoofing. The extremely high redundancy of the network is another powerful measure against data spoofing from any site because strong majority voting schemes can be employed to detect any anomalous sites. Processing to estimate the TEC value needs to consider some biases (influences) during the restoration of the TEC values from the measurements of the dual-frequency delays of the GPS signals, which are associated with the cycle slips, resolution of carrier phase ambiguity, determination of hardware delays for the phases, code measurements, and tropospheric and multipath problems. The Kalman filter is used to estimate the TEC with less bias [39]. Kalman filter is an algorithm, and using this filter, a series of data measurements containing noise and other inaccuracies are observed over time. It corrects observed data to more accurate forms than those based on a single measurement alone by estimating a joint probability distribution over the observed data for each timeframe.

III. K2DPCA

For the K2DPCA, a brief introduction is as follows;

(a) Let the input signals be represented by matrix W (whose dimensions are of the form $n \times m$, where $n \leqq m$). However, when W is not a square matrix with dimension $m \times n$, it must be transposed to W^T with dimension n × m, where T implies ''transpose''. This is necessary to allow the K2DPCA the advantage of increasing computing speed. The nonlinear projection of the form is considered as follows [58], [22]:

$$(b)\ B = \Psi(W)A. \tag{1}$$

Here, A is an n-dimensional project axis, and B is the projected feature (matrix) of the signals on vectors $a_1, a_2 \cdots a_n$, which are called the principal-component vectors with the number of n. Ψ is defined as Gaussian Radial Basis function (RBF) kernel.

$$(c)\ C = E(\Psi(B) - \Psi(EB))(\Psi(B) - \Psi(EB))^T \tag{2}$$

where E is the norm in Euclidean space and is called the Euclidean norm.

(d) C is the covariance matrix of the project feature vector.

(e) The trace of C is defined as follows;

$$tr(C) = \Psi(A)^T F \Psi(A), \tag{3}$$

where

$$F = E[(\Psi(W) - \Psi(EW))^T(\Psi(W) - \Psi(EW))] \tag{4}$$

(f) Matrix F is called the signal covariance matrix.

(g) The vectors $a_1, a_2 \cdots a_n$, which maximize (4), correspond to the principal eigenvalue of F and therefore result in n principal eigenvalues $\lambda_1, \lambda_2 \cdots \lambda_n$ corresponding to the vectors of $a_1, a_2 \cdots a_n$. Each principal eigenvalue corresponds to a vector.

(h) Each principal eigenvalue represents a certain class of data characteristics. Therefore, the entire characteristics of the data can be represented using n principal eigenvalues from largest to smallest magnitude. In this study, the principal eigenvalue with the largest magnitude is called the first principal eigenvalue λ_1. The principal eigenvalue with the smallest magnitude is called the principal eigenvalue λ_n. Therefore $\lambda_1 > \lambda_2 > \ldots > \lambda_n$ is indicated.

As stated previously, instead of PCA, 2DPCA belongs to Generalized 2D principal component analysis. It can be used to reduce high-dimensional 2D data into the low-dimensional

matrix of principal eigenvalues without distorting data processing, despite it being a linear method. Another advantage of 2DPCA is to solve the problem of 2D TEC data that has a small sample signal size (SSS), without distorting data processing. K2DPCA also belongs to Generalized 2D principal component analysis, which is a nonlinear method. It can also solve the SSS problem in non-linear 2D TEC data [58], [22].

PCA is a suitable tool for processing of one-dimensional (1D) TEC data. However, the PCA and KPCA convert the measurements into 1D TEC data before the covariance matrix calculation [58]. The covariance matrixes of PCA and KPCA are based on an input matrix with a dimension of $n \times m$, which is reshaped from 1D data (length of m multiplied by n) to form the matrix with a rank of n rows and m columns. Reshaping of the data into 2D data will cause data-processing error, especially in reshaping small matrices [23]. Such processing means that the spatial structure and information cannot be well preserved because of some original information loss during the inversion to the original dimension when the matrix has a small SSS. As previously stated, a similar concept of image processing, which is dividing the images into subimages called tiles, will cause a large image-processing error when the subimage is very small [4]. Such processing-information loss is also called an SSS problem. It is suitable to solve the problem of large data processing errors with low-spatial-resolution ionospheric TEC data, which form the low-dimension matrix, to reduce the errors. These errors may estimate incorrect principal eigenvalues, which cause misjudgment as false TEC precursors. Therefore, the SSS problem due to processing-information loss can be avoided. Thus, the covariance matrix of the K2DPCA is a full-rank matrix with a low dimension, which does not require reshaping of the 1D data. Therefore, the curse of dimensionality and SSS problems can be avoided [22]. In the current study, all principal eigenvalues of K2DPCA and 2DPCA are used to represent the entire characteristics of the data, and we attempt to find other TEC precursors associated with the same earthquake. The results of K2DPCA will be compared with the results of 2DPCA.

IV. TEC DATA PROCESSING

The 2DPCA and K2DPCA are used to determine an ionospheric 2D TEC precursor using the TEC data, which occurred five days before this earthquake [30]. However, two TEC precursors prior to the earthquake were observed during 06:15–06:20 UT on August 1, 2014. Therefore, processing during this period is used in the present study. Fig. 1 shows the GIM during 06:15–06:20 UT on August 1, 2014. The TEC data of the global region (GIM was not divided for image processing) shown in Fig. 1 are divided into 600 smaller areas. The size of each small area is 12° in longitude and 9° in latitude. This size is reasonable for examination of the of unknown focus size, and the spatial resolution of the TEC data can support examination of an entire TEC abnormal variation related to earthquakes over the epicenter area. As presented in the study of [50], the estimated epicenter area of these investigated earthquakes was $\approx \times 5°$. The size of the small area was larger than the estimated epicenter area. The choice of the area size depended on the focus size and spatial resolution of the TEC data, as previously stated. Therefore, fine TEC abnormal variations can be detected in principle. We need to mention that the area size can be very small when the spatial resolution of the TEC data is fine. The epicenter area is very small, and thus, more fine TEC abnormal variations can be detected. However, earthquake precursors toned to be considered in this study to belong to the earthquake-prediction problem, and detailed TEC feature does not need to be considered as its scope.

The spatial resolution values of the TEC data for GDGPS are 5° and 2.5° in longitude and latitude, respectively [15]. Therefore, the GDGPS data are suitable for examination of the TEC variation to detect TEC precursors, and the TEC data processing is not complicated. In the present study, four TEC data points (2D data) are considered in each area. The TEC data form matrix W, as expressed in (1), with a dimension of 2×2, as a small SSS data in each area and results in two principal eigenvalues: $\lambda_1 > \lambda_2$. All the principal eigenvalues of 2DPCA and K2DPCA are shown in Figs. 2, 3, 4 and 5. The first and second principal eigenvalues are computed for each of the 600 smaller areas. These principal eigenvalues are a result of the feature scaling between zero and one [28].

V. RESULTS

The first and second principal eigenvalues of 2DPCA and K2DPCA are shown in Figs. 2, 3, 4 and 5 for comparisons, respectively. They indicate the existence of TEC precursors represented by the characteristics of the two largest principal eigenvalues. However, the second largest principal eigenvalue, which is a TEC precursor that occurred far west of the epicenter, was similar to that obtained by [62]. We must mention that this phenomenon was not a co-seismic ionospheric effect after an earthquake caused by the acoustic-gravity waves [61]. Other non-earthquake TEC anomalies, such as the equatorial ionization anomaly (EIA) shown in Figure 1, are therefore suppressed by the largest principal eigenvalues, which are defined as TEC precursors in other examined periods in the present study. Therefore, the result of this study also proves the detection of TEC precursors without considering the influence of other non-earthquake TEC anomalies. The results obtained by Lin (2014 and 2016) have also proven the absence of influence on the other non-earthquake TEC anomalies. K2DPCA has improved the identification of detecting TEC precursors. On the other hand, K2DPCA could detect TEC precursors with higher resolution than those of 2DPCA i.e. clearer TEC precursors from Figs. 4 and 5.

The possibility of other factors such as solar flares and geomagnetic effects to affect the results are considered by examining the Kp indexes shown in Fig. 6. Kp is calculated as a weighted average of the K indexes from a network of geomagnetic observatories. The Kp index allows the disturbances in the horizontal component of the Earth magnetic field to be represented on a scale of zero to nine, with one being calm and

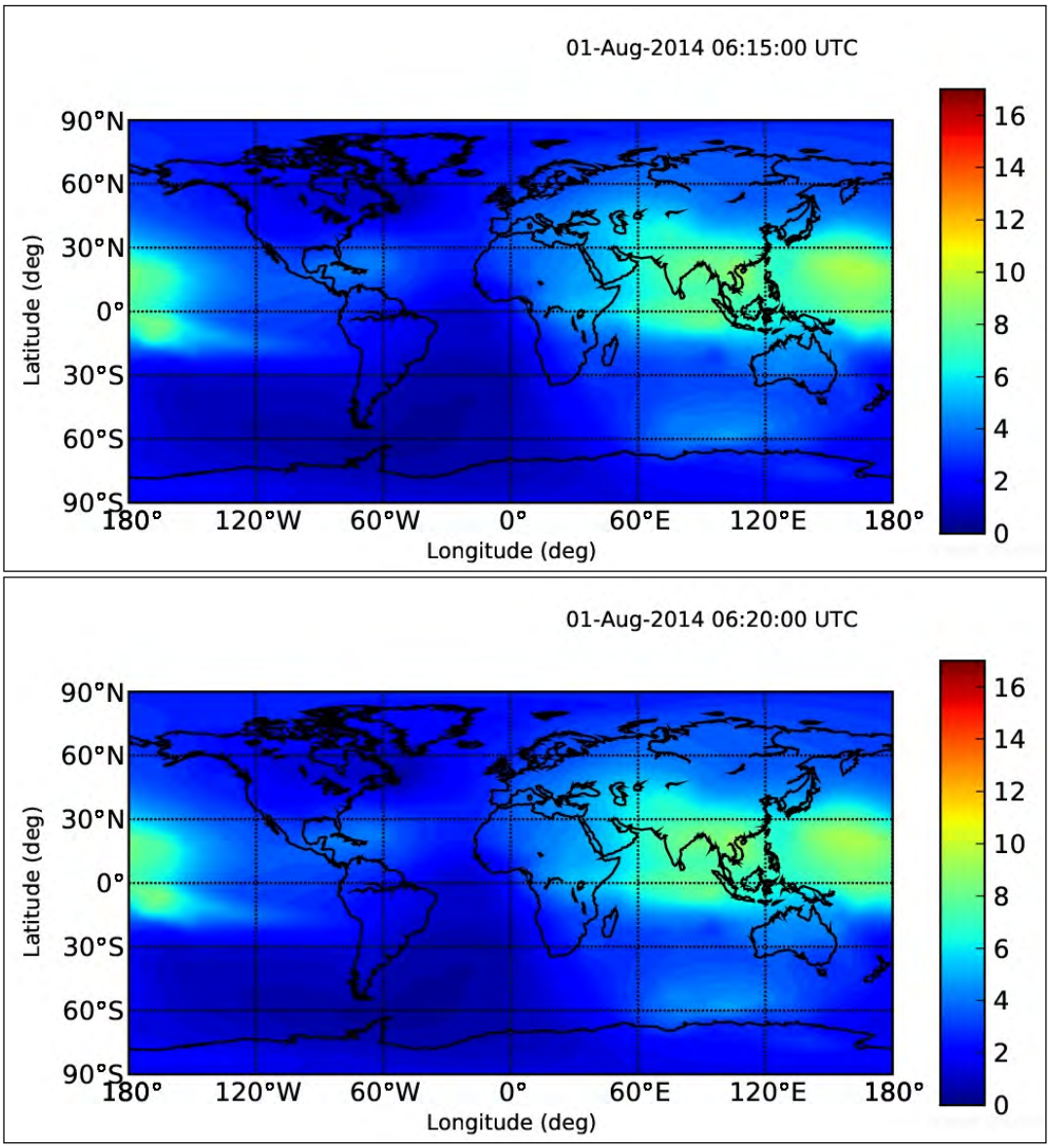

FIGURE 1. The global ionospheric map (GIM) for 06:15 to 06:20 UT on 01 August 2014. The equatorial ionization anomaly (EIA) lies within approximately ± 30 degrees of the magnetic equator.

five or higher indicating a geomagnetic storm. August 1 was a geomagnetically quiet day, as shown in Fig. 6 (Kp < 4) [53]. However, as previously stated, the PCA method was shown to be independent of the geomagnetic situation and other non-earthquake TEC anomalies. Examination of a geomagnetically quiet day might be unnecessary [25] to prove the results of K2DPCA, which were not affected by a geomagnetic storm. Figure 7 shows the GIM at 00.00 on August 6, 2011 and corresponding principal eigenvalues of the K2DPCA.

Figure 8 shows the corresponding *Dst* indices (The *Dst* index indicates geomagnetic effects as per the *Kp* index) for the first and second principal eigenvalues. The influence of geomagnetic storms with respect to principal eigenvalues of small magnitude should be excluded in this study.

VI. DISCUSSION

The 2DPCA and K2DPCA were able to detect two precursors using the characteristics of the first and second largest principal eigenvalues in the China's Ludian earthquake from 06:15 to 06:20 UT on August 1, 2014, three days prior to the earthquake. The benefit of this analysis was that the nonlinear method could be applied to process nonlinear data. With similar results, [60] described the TEC anomalies that were observed one to three days before the Ludian earthquake. Although the causal mechanisms of the TEC anomalies were not fully understood, a multiple-parameter examination can increase the credibility of the determination regarding the pre-earthquake phenomena, including radon-gas release. No significant anomalies could be found using the electromagnetic data. As previously stated, according

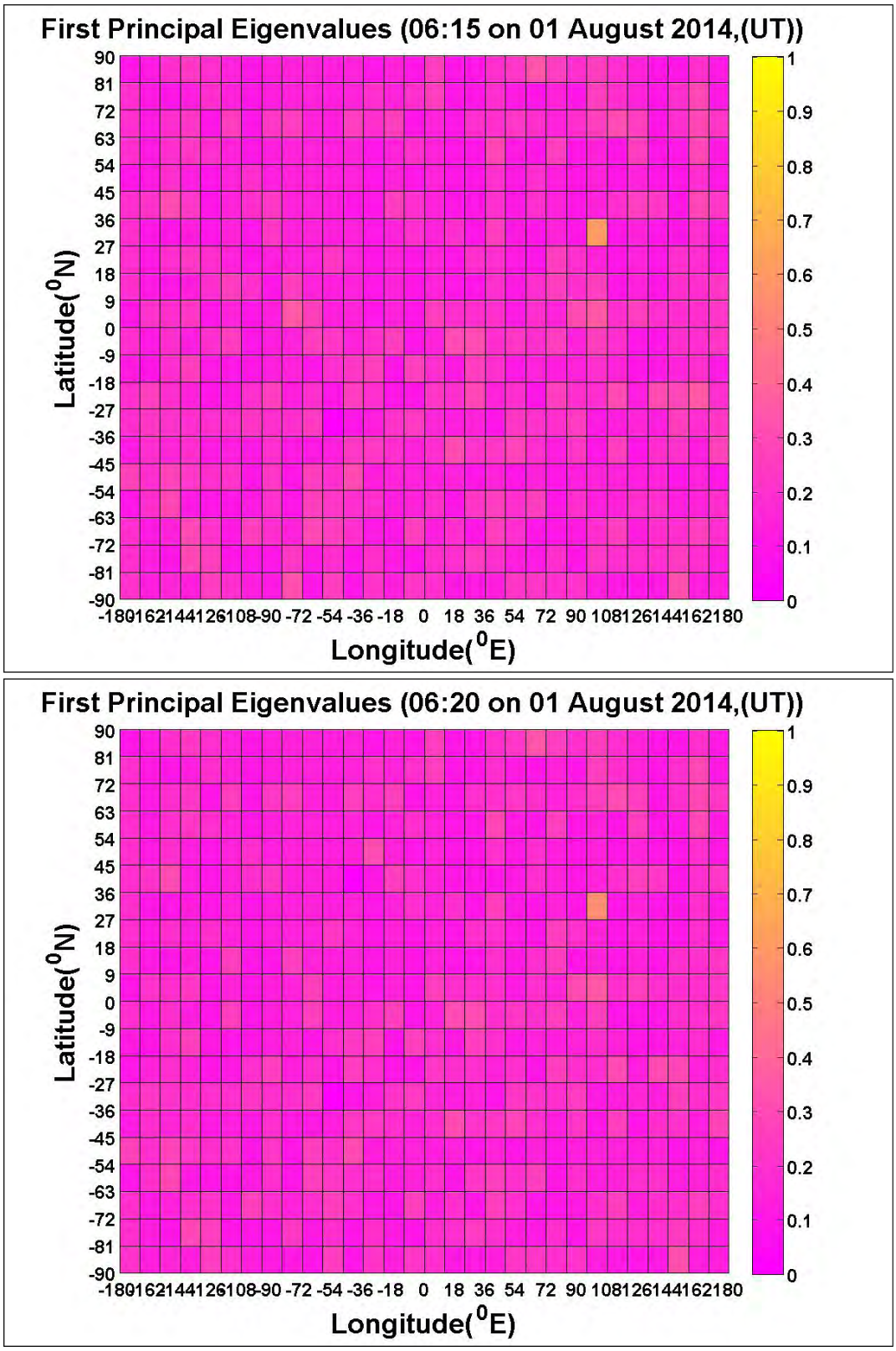

FIGURE 2. Color-coded scale of the magnitudes of the first principal eigenvalues of the 2DPCA. The color within an area denotes the magnitude of the principal eigenvalue; thus, 600 principal eigenvalues are assigned.

to the geological conditions, the first possible cause was the heat-flux changes or transfers immediately before the earthquake, which enhanced the temperature of the soil and groundwater of the local area causing a release of radon gas at

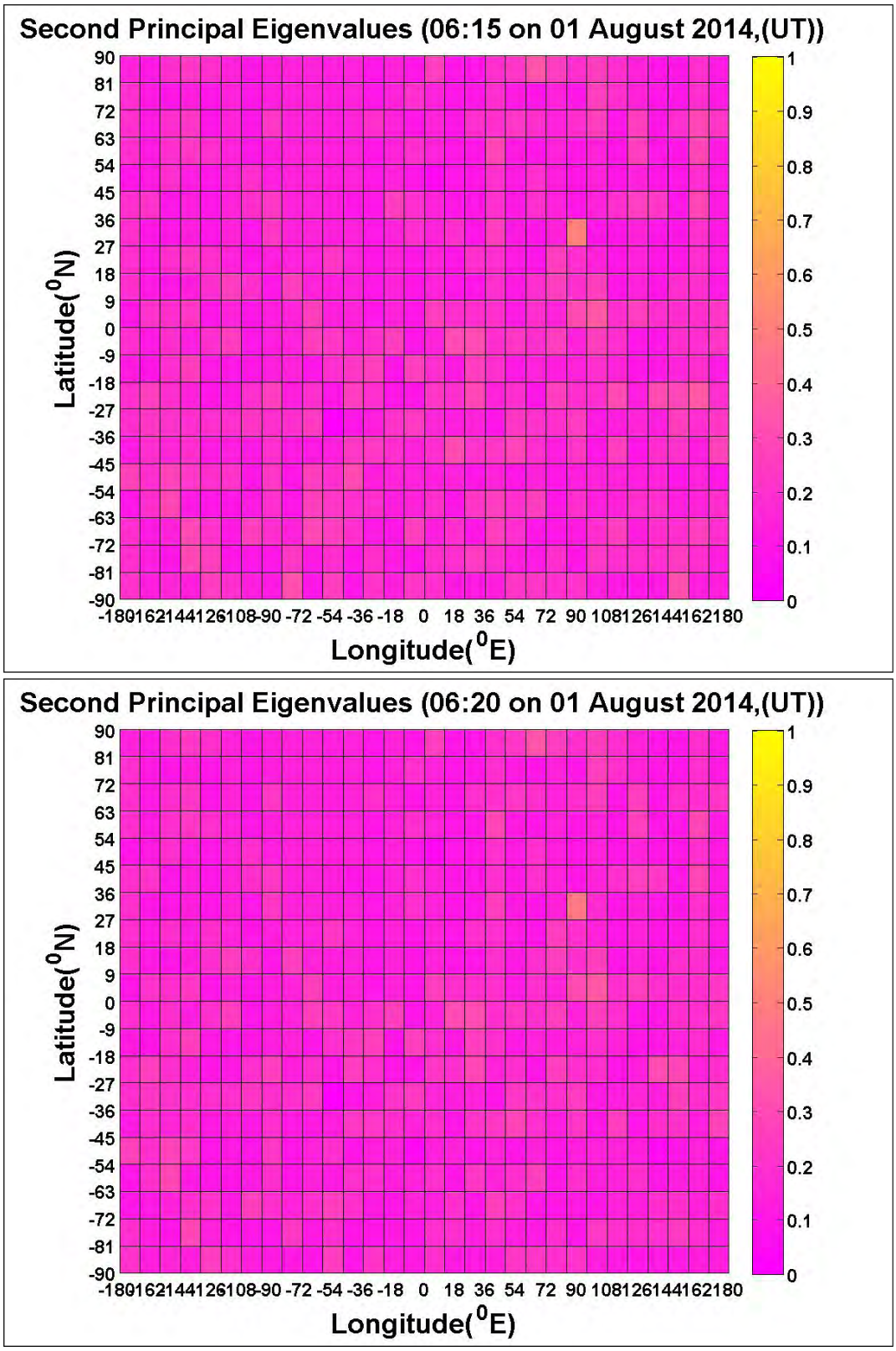

FIGURE 3. Color-coded scale of the magnitudes of the second principal eigenvalues of the 2DPCA related to Fig. 2.

a site far to the west of the epicenter in Ludian. The TEC precursors of this study, which are born of a release of radon gas, were also confirmed using continuous MODIS/Terra satellite remote sensing thermal infrared data of the earthquake

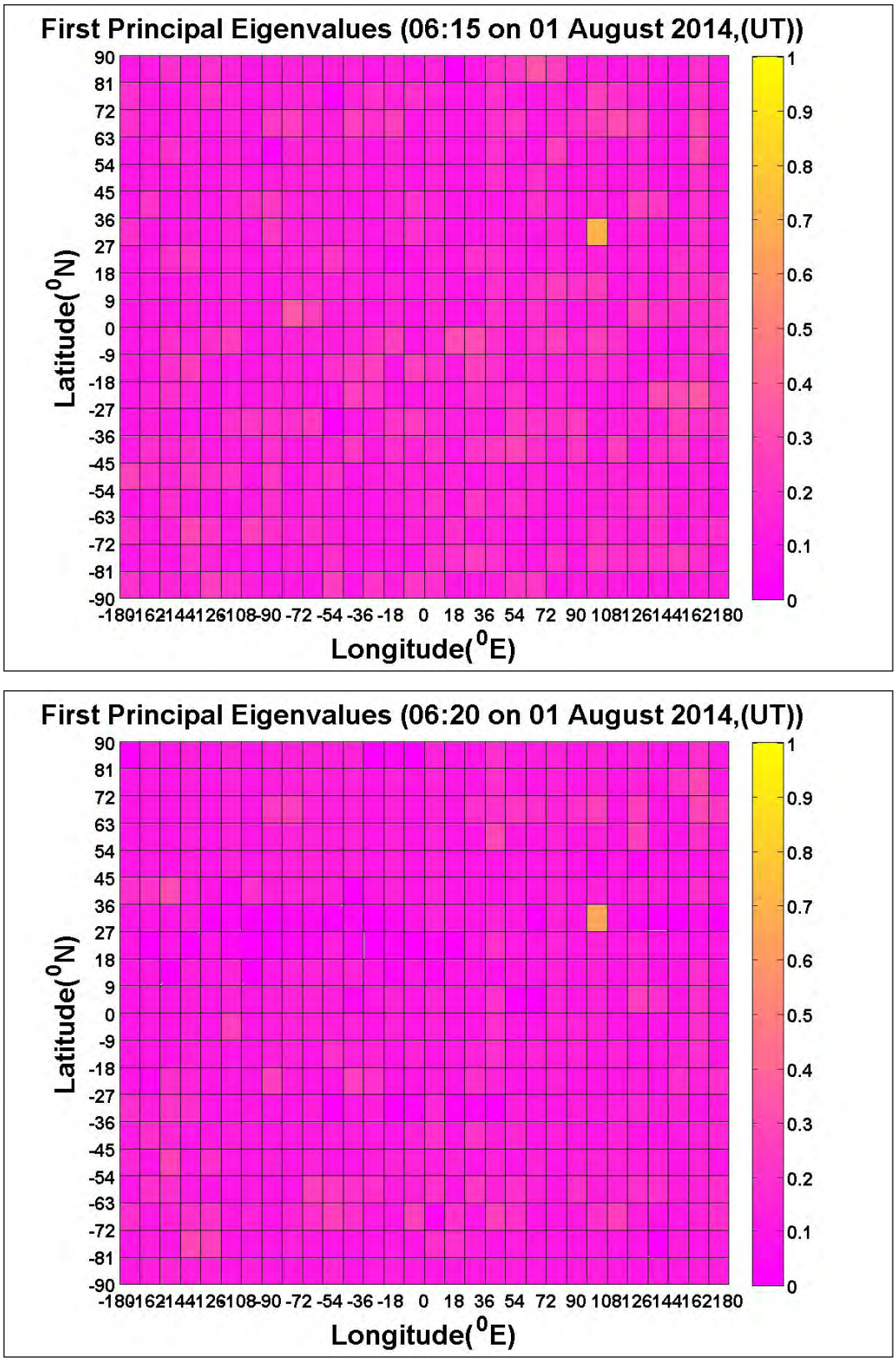

FIGURE 4. Color-coded scale of the magnitudes of the first principal eigenvalues of the K2DPCA. The color within an area denotes the magnitude of the principal eigenvalue; thus, 600 principal eigenvalues are assigned.

region in Ludian for June to August 2014; this data was obtained from the study by [57]. The second possible reason was that the fault related to the earthquake had a slight real-time activity before the earthquake, which triggered fine

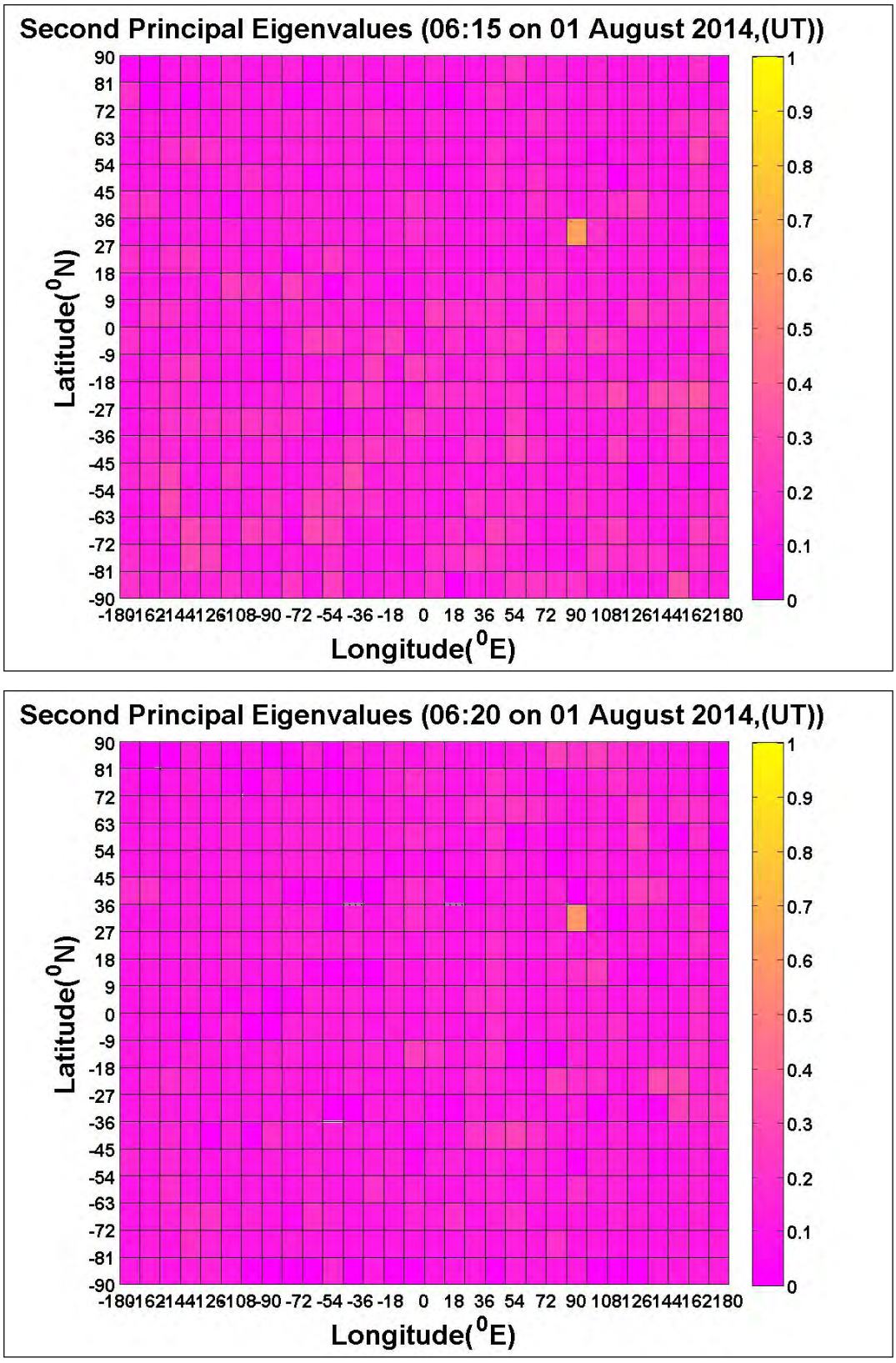

FIGURE 5. Color-coded scale of the magnitudes of the second principal eigenvalues of the K2DPCA related to Fig. 4.

cracks (microfractures) in the local rock accompanied with the soil and groundwater according to the Coulomb stress transfer theory [2], [56]. This process emanated radon gas eastwards from a site far west of the fault. The third possible

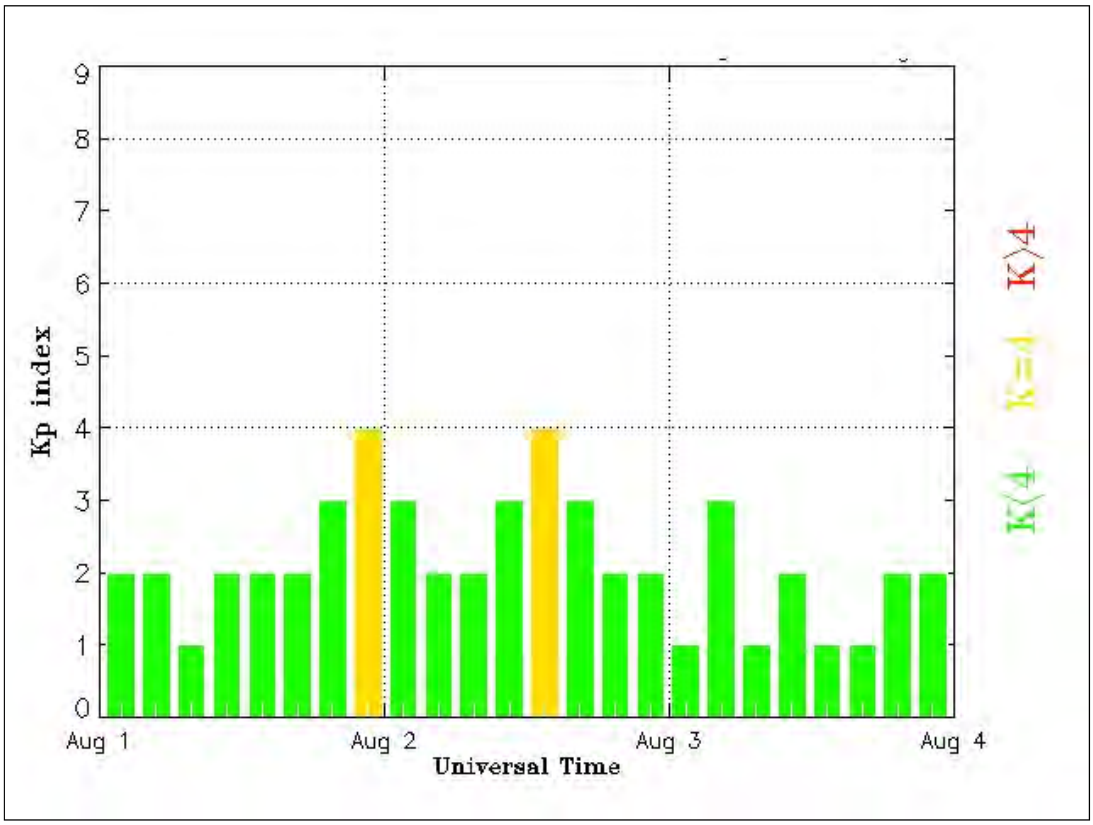

FIGURE 6. *Kp* indexes from August 1 to 3, 2014.

reason is that the TEC variations resulting in horizontally propagating disturbances spreading from the epicenter area in the ionosphere were considered [9].

However, from the occurrence time of the two TEC precursors shown in Figs. 2, 3, 4 and 5 the second reason was a reasonable explanation because the rock-stress transfer occurred in real time according to the Coulomb stress transfer theory [2], [56].

Reference [62] investigated the Wenchuan earthquake on May 12, 2008 with ML $=$ 8.0, and its epicenter center was located in southwest China (31.0° N, 103.4° E). The maximum ionospheric electron density showed an unusual large enhancement during sunset, as recorded by the Chinese ionosondes over Wuhan (30.5° N, 114.4° E) and Xiamen (24.4° N, 123.9° E). The TEC anomaly was close to the earthquake epicenter. Another TEC anomaly was observed far from the epicenter. The average increase in these two stations approximately occurred on a geomagnetically quiet day, May 9, 2008 ($Kp \leq 2$), which was three days prior to the earthquake. Reference [11] also suggested that most TEC precursors of earthquakes were due to radon-gas release in the Ludian region. Identifying the precise cause of TEC precursors is not easy. One reason is the number of potential causes of TEC precursors that arise during earthquake preparation, the main shock, and the aftershocks. For example, during the earthquake-generation phase, [43] suggested that radon gas that emanates from active faults and crust-rock cracks before earthquakes ionizes the near-ground atmosphere to produce large vertical electric fields. Reference [7] proposed that mobile positive holes in the Earth crust could be activated by low-energy impact, sound waves, and microfractures, creating charge clouds that could explain the electromagnetic activity. Gravity waves that arise from fine vibrations in the Earth surface leading to radon-gas release are another possibility. These waves result in lower atmospheric turbulence and eventual ionospheric perturbations [37]. However, once an earthquake occurs, the most evident physical mechanism is the radon gas that emanates from active faults of soil, groundwater, and rock cracks before earthquakes, which ionizes the near-ground atmosphere to produce large vertical electric fields. Then, the presence of an electric field causes large-scale ionospheric density irregularities [42] coupled with potential drift in the anomaly toward the equator. However, this anomaly resembles what we would expect from rising acoustic gravity waves due to strong motion. As discussed in the Introduction, the Earth atmosphere could act as a natural amplifier because of the decline in the atmospheric density with height.

Therefore, the scientific contributions of this study are as follows. (1) The TEC precursors can be detected by understanding the TEC conditions. (2) This method is independent of the TEC variation from the effects of space weather

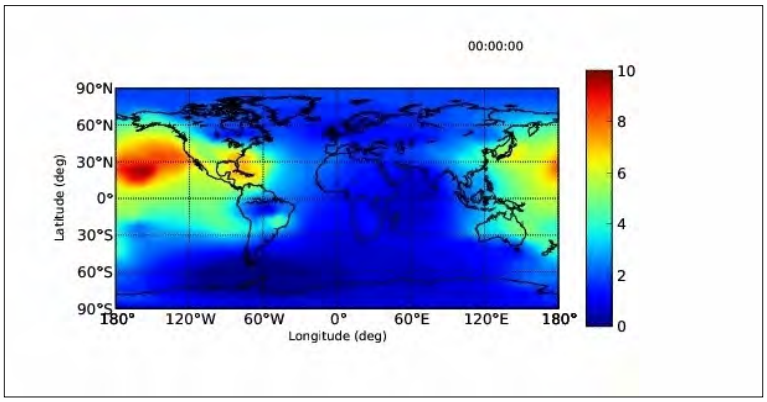

(a)

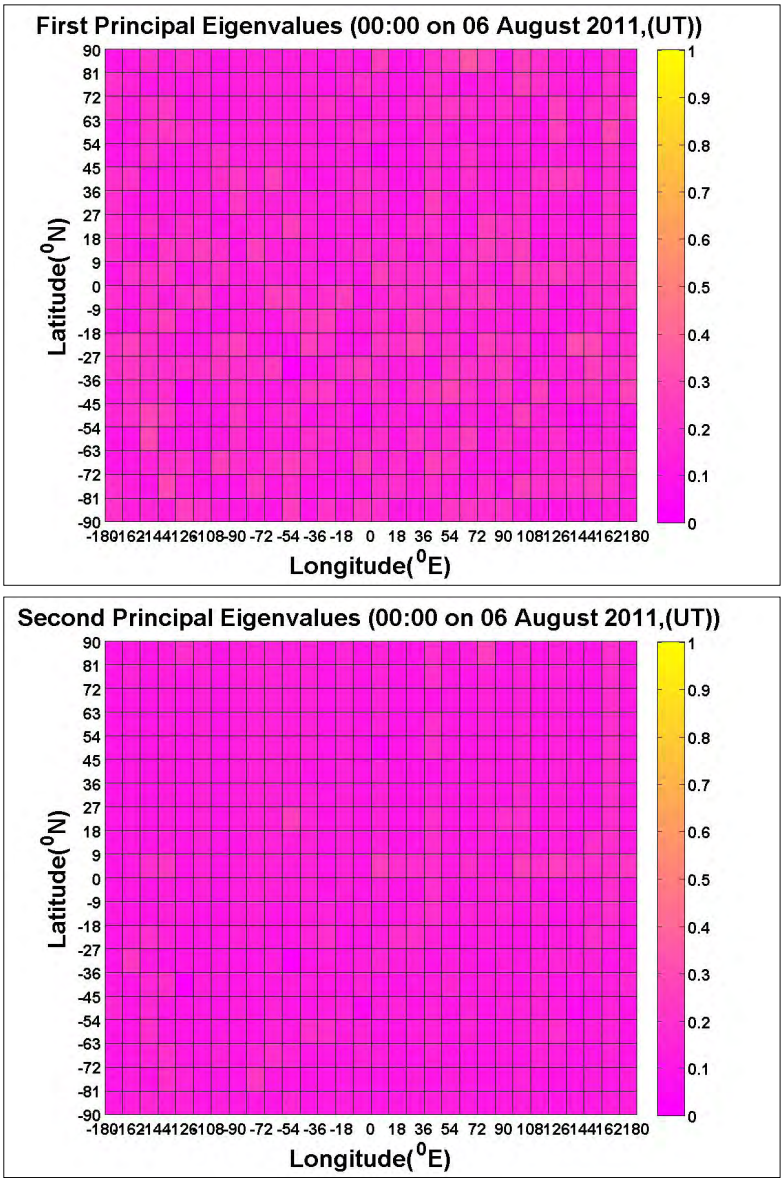

(b)

FIGURE 7. (a) GIM at 00:00 UT on August 6, 2011 (Lin, 2012). (b) Color-coded scale for the magnitudes of the first and second principal eigenvalues of the K2DPCA corresponding to (a).

and other non-earthquake TEC anomalies, as shown by the results of Lin's studies (2014, 2016). Therefore, the studies by Lin (2014, 2016) and this study, via the detection of TEC precursors, have shown that principal eigenvalues

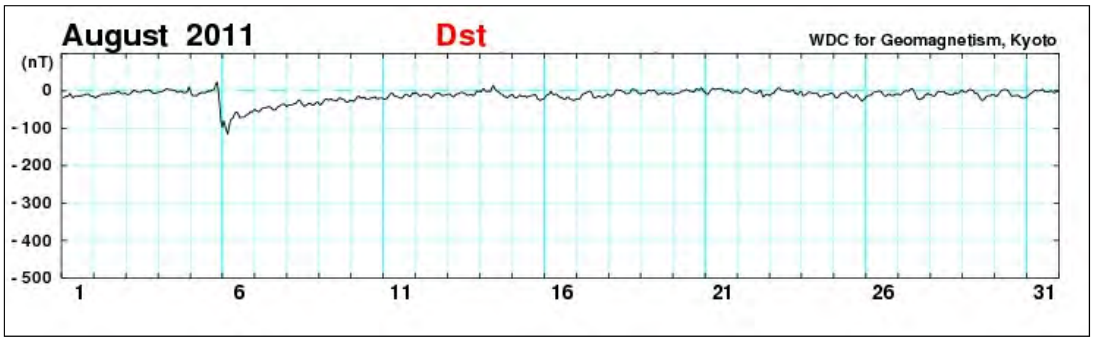

FIGURE 8. The Dst indices for August 2011 (Lin, 2012).

could undoubtedly serve as indicators of TEC precursors. (3) In this study, a TEC precursor could be found far to the west of the epicenter using the second largest principal eigenvalue. This is unlike the studies by Lin (2014, 2016), where only the first largest principal eigenvalue was used and only the TEC precursors near the epicenter were detected. (4) The TEC precursors prior to earthquakes through radon-gas release in Ludian could be a possible factor, as indicated by the results of [57] and [11] studies.

Finally, the largest principal eigenvalue is only a mathematical indicator that indicates the TEC precursors. In this study, a TEC precursor was found far west of the epicenter. However, the actual TEC spread distance, variants, and speed of the TEC precursors might be difficult to obtain, which is a limitation of this study. In future research, the physical meaning of principal eigenvalue should be understood so that the actual properties of TEC precursors can be reflected through the characteristic of principal eigenvalues.

When TEC variants caused by earthquakes are concentrated on a small part of the area, then these TEC variants may be not easy to estimate using K2DPCA under the condition of low spatial resolution ionospheric TEC data, which is a limitation of this study. Nevertheless, for the purpose of predicting TEC precursors, the low spatial resolution ionospheric TEC data used in this study were adequate. Solving the problem of large data processing errors with low ionospheric spatial resolution TEC data is an advantage of K2DPCA when high ionospheric spatial resolution TEC data cannot be easily obtained.

VII. CONCLUSION

In this study, 2DPCA and K2DPCA were simultaneously used to detect two TEC precursors during the three days prior to earthquake occurrence via the characteristics of the first and second eigenvalues. The results showed that the two TEC precursors were detected from 06:15 to 06:20 UT. However, one of the TEC precursors was located far west of the epicenter. The two TEC precursors might be indicative of radon gas release that could cause TEC density variations because of the transfer stress of fine cracks, according to Coulomb stress transfer theory as applied to a far TEC precursor. The duration of these TEC precursors were at least 5 min. This study can be considered as a detailed examination and analysis of the surrounding TEC precursors related to earthquakes. Two TEC precursors were clearer using K2DPCA.

ACKNOWLEDGEMENTS

The author is grateful to: NASA Global Differential GPS system (GDGPS), U.S. Geological Survey and Central Weather Bureau (CWB) in Taiwan for their useful references Data and the parameters of this earthquake. This work was supported by Ministry of Science and Technology, Taiwan, Grant MOST 106-2221-E-218 -001 -MY2. Especially, in Memory of death to the mother of first author, ''Lo, Yu-Mei'' (8 Nov 1943 - at am: 5:44 on 9 Oct 2016). Also thank you for the Lover ''Yang, Yu-Chen'' of first author.

REFERENCES

[1] M. Akhoondzadeh, A. De Santis, D. Marchetti, A. Piscini, and G. Cianchini, ''Multi precursors analysis associated with the powerful Ecuador (M_W = 7.8) earthquake of 16 April 2016 using Swarm satellites data in conjunction with other multi-platform satellite and ground data,'' *Adv. Space Res.*, vol. 61, no. 1, pp. 248–263, 2018. doi: 10.1016/j.asr.2017.07.014.

[2] Z. Bei, H.-H. Cheng, and Y.-L. Shi, ''Calculation of co-seismic effects of the nepal M_S8.1 earthquake on 25 April 2015,'' *Chin. J. Geophys.*, vol. 58, no. 3, pp. 269–279, 2015. doi: 10.1002/cjg2.220172.

[3] B. Bhaskar, P. S. Anushree, S. D. Shree, and K. V. M. Prashanth, ''Quantitative analysis of kernel principal components and kernel Fishers based face recognition algorithms using hybrid Gaborlets,'' *Procedia Comput. Sci.*, vol. 58, pp. 342–347, 2015. doi: 10.1016/j.procs.2015.08.029.

[4] N. Biyani, S. Scherer, R. D. Righetto, J. Kowal, M. Chami, and H. Stahlberg, ''Image processing techniques for high-resolution structure determination from badly ordered 2D crystals,'' *J. Struct. Biol.*, vol. 203, no. 2, pp. 120–134, 2018. doi: 10.1016/j.jsb.2018.03.013.

[5] W. B. Cade, III, and C. Chan-Park, ''The origin of 'space weather,''' *Space Weather*, vol. 13, no. 2, pp. 99–103, 2015. doi: 10.1002/2014SW001141.

[6] C. Chen and K. Xie, ''Face recognition based on two-dimensional principal component analysis and kernel principal component analysis,'' *Inf. Technol. J.*, vol. 11, no. 12, pp. 1781–1785, 2012. doi: 10.3923/itj.2012.1781.1785.

[7] F. Freund, ''Time-resolved study of charge generation and propagation in igneous rocks,'' *J. Geophys. Res.*, vol. 105, no. B5, pp. 11001–11019, 2000. doi: 10.1029/1999JB900423.

[8] F. T. Freund, ''Rocks that crackle and sparkle and glow: Strange pre-earthquake phenomena,'' *J. Sci. Explor.*, vol. 17, no. 1, pp. 37–71, 2003. doi: 10.1.1.465.8324.

[9] D. Gómez *et al.*, ''Virtual array beamforming of GPS TEC observations of coseismic ionospheric disturbances near the Geomagnetic South Pole triggered by teleseismic megathrusts,'' *J. Geophys. Res. Space Phys.*, vol. 120, no. 10, pp. 9087–9101, 2015. doi: 10.1002/2015JA021725.

[10] S.-I. Goto, R. Uchida, K. Igarashi, C.-H. Chen, M. Kao, and K. Umeno. (2018). ''Pre-seismic ionospheric anomalies detected before the 2016 Taiwan earthquake.'' [Online]. Available: https://arxiv.org/abs/1806.03782. doi: 10.13140/RG.2.2.10100.65922.

[11] F. Huang *et al.*, "Studies on earthquake precursors in China: A review for recent 50 years," *Geodesy Geodyn.*, vol. 8, no. 1, pp. 1–12, 2017. doi: 10.1016/j.geog.2016.12.002.

[12] K. Hattori, S. Hirooka, M. Kunimitsu, T. Ichikawa, and P. Han, "Ionospheric anomaly as an earthquake precursor: Case and statistical studies during 1998–2012 around Japan," in *Proc. 31st URSI Gen. Assem. Sci. Symp. (URSI GASS)*, 2014, p. 1. doi: 10.1109/URSIGASS.2014.6929866.

[13] K. Heki and Y. Enomoto, "M_w dependence of the preseismic ionospheric electron enhancements," *J. Geophys. Res.*, vol. 120, no. 8, pp. 7006–7020, 2015. doi: 10.1002/2015JA021353.

[14] L. He and K. Heki, "Three-dimensional tomography of ionospheric anomalies immediately before the 2015 illapel earthquake, central chile," *J. Geophys. Res.*, vol. 123, no. 5, pp. 4015–4025, 2018. doi: 10.1029/2017JA024871.

[15] M. Hernández-Pajares *et al.*, "The IGS VTEC maps: A reliable source of ionospheric information since 1998," *J. Geodesy*, vol. 83, nos. 3–4, pp. 263–275, 2009. doi: 10.1007/s00190-008-0266-1.

[16] B. Hofmann-Wellenhof, H. Lichtenegger, and J. Collins, *Global Positioning System: Theory and Practice*. Vienna, Austria: Springer, 2001, p. 382. doi: 10.1007/978-3-7091-6199-9.

[17] T. Iwata and K. Umeno, "Preseismic ionospheric anomalies detected before the 2016 Kumamoto earthquake," *J. Geophys. Res.*, vol. 122, no. 3, pp. 3602–3616, 2017. doi: 10.1002/2017JA023921.

[18] T. X. Jiang, T. Z. Huang, X. L. Zhao, and T. H. Ma, "Patch-based principal component analysis for face recognition," *Comput. Intell. Neurosci.*, vol. 2017, 2017, Art. no. 5317850. doi: 10.1155/2017/5317850.

[19] S. Kalita, M. Devi, A. K. Barbara, and P. H. Talukdar, "Soft computing technique for recognition of earthquake precursor from low latitude total electron content (TEC) profiles," *Int. J. Comput. Appl.*, vol. 44, no. 17, pp. 11–14, 2012. doi: 10.5120/6354-8775.

[20] S. Kalita, "Monitoring the TEC variation using pattern matching method during earthquakes as determined from ground based TEC measurement and satellite data," *Int. J. Sci. Res. Publications*, vol. 5, no. 6, p. 4, 2015.

[21] S. P. Karia, K. N. Pathak, K. S. Yadav, N. P. Chaudhary, N. C. Patel, and R. Jana, "Modification in atmospheric refractivity and GPS based TEC as earthquake precursors," *Positioning*, vol. 5, no. 2, 2014, Art. no. 46156. doi: 10.4236/pos.2014.52006.

[22] H. Kong, L. Wang, E. K. Teoh, X. Li, J.-G. Wang, and R. Venkateswarlu, "Generalized 2D principal component analysis for face image representation and recognition," *Neural Netw.*, vol. 18, nos. 5–6, pp. 585–594, 2005. doi: 10.1016/j.neunet.2005.06.041.

[23] M. A. Kramer, "Nonlinear principal component analysis using autoassociative neural networks," *AIChE J.*, vol. 37, no. 2, pp. 233–243, Feb. 1991. doi: 10.1002/aic.690370209.

[24] W. Li, J. Yue, J. Guo, Y. Yang, B. Zou, Y. Shen, and K. Zhang, "Statistical seismo-ionospheric precursors of M7.0+ earthquakes in Circum-Pacific seismic belt by GPS TEC measurements," *Adv. Space Res.*, vol. 61, no. 5, pp. 1206–1219, 2018. doi: 10.1016/j.asr.2017.12.013.

[25] J.-W. Lin, "Ionospheric total electron content seismo-perturbation after Japan's March 11, 2011, M =9.0 Tohoku earthquake under a geomagnetic storm; A nonlinear principal component analysis," *Astrophys. Space Sci.*, vol. 341, no. 2, pp. 251–258, 2012. doi: 10.1007/s10509-012-1128-0.

[26] J.-W. Lin, "Ionospheric precursor of 2008 China Wenchuan earthquake using two-dimensional principal component analysis," *HKIE Trans.*, vol. 21, no. 3, pp. 192–194, 2014. doi: 10.1080/1023697X.2014.944876.

[27] L. Jyh-Woei, "Detecting ionospheric anomalies associated with three Japan Miyako earthquakes to show their correlations and associated earthquake-induced tsunamis," *Geodesy Cartography*, vol. 42, no. 1, pp. 7–15. 2016. doi: 10.3846/20296991.2016.1168017.

[28] J.-W. Lin, C.-T. Chao, and J.-S. Chiou, "Determining neuronal number in each hidden layer using earthquake catalogues as training data in training an embedded back propagation neural network for predicting earthquake magnitude," *IEEE Access*, vol. 6, pp. 52582–52597, 2018. doi: 10.1109/ACCESS.2018.2870189.

[29] O. Lindenbaum, Y. Bregman, N. Rabin, and A. Averbuch, "Multiview kernels for low-dimensional modeling of seismic events," *IEEE Trans. Geosci. Remote Sens.*, vol. 56, no. 6, pp. 3300–3310, Jun. 2018. doi: 10.1109/TGRS.2018.2797537.

[30] J. Y. Liu, Y. I. Chen, Y. J. Chuo, and C. S. Chen, "A statistical investigation of preearthquake ionospheric anomaly," *J. Geophys. Res.*, vol. 111, no. A5, 2006, Art. no. A05304. doi: 10.1029/2005JA011333.

[31] J. Y. Liu *et al.*, "Seismoionospheric GPS total electron content anomalies observed before the 12 May 2008 M_w7.9 Wenchuan earthquake," *J. Geophys. Res.*, vol. 114, no. A4, 2009, Art. no. A04320. doi: 10.1029/2008JA013698.

[32] J.-Y. Liu, C.-H. Chen, C.-H. Lin, H.-F. Tsai, C.-H. Chen, and M. Kamogawa, "Ionospheric disturbances triggered by the 11 March 2011 M9.0 Tohoku earthquake," *J. Geophys. Res.*, vol. 116, no. A6, 2011, Art. no. A06319. doi: 10.1029/2011JA016761.

[33] F. Masci, J. N. Thomas, F. Villani, J. A. Secan, and N. Rivera, "On the onset of ionospheric precursors 40 minbefore strong earthquakes," *J. Geophys. Res. Space Phys.*, vol. 120, no. 2, pp. 1383–1393, 2015. doi: 10.1002/2014JA020822.

[34] D. J. McComas, H. A. Elliott, N. A. Schwadron, J. T. Gosling, R. M. Skoug, and B. E. Goldstein, "The three-dimensional solar wind around solar maximum," *Geophys. Res. Lett.*, vol. 30, no. 10, p. 1517, 2003. doi: 10.1029/2003GL017136.

[35] N. Meyer-Vernet, *Basics of the Solar Wind* (Cambridge Atmospheric and Space Science Series). Cambridge, U.K.: Cambridge Univ. Press, 2012, p. 480.

[36] R. W. Middlestead, *Ionospheric Propagation*. Hoboken, NJ, USA: Wiley, 2017, ch. 20, pp. 824. doi: 10.1002/9781119011866.

[37] O. A. Molchanov and M. Hayakawa, "Subionospheric VLF signal perturbations possibly related to earthquakes," *J. Geophys. Res.*, vol. 103, no. 8, pp. 17489–17504, 1998. doi: 10.1029/98JA00999.

[38] C. Oikonomou, H. Haralambous, and B. Muslim, "Investigation of ionospheric TEC precursors related to the M7.8 Nepal and M8.3 Chile earthquakes in 2015 based on spectral and statistical analysis," *Natural Hazards*, vol. 83, pp. 97–116, Oct. 2016. doi: 10.1007/s11069-016-2409-7.

[39] G. Ouyang, J. Wang, J. Wang, and D. Cole, "Analysis on temporal-spatial variations of Australian TEC," in *Observing our Changing Earth*. 2009, pp. 751–758. doi: 10.1007/978-3-540-85426-5_86.

[40] L. Perrone *et al.*, "Ionospheric anomalies detected by ionosonde and possibly related to crustal earthquakes in Greece," *Ann. Geophys.*, vol. 36, no. 2, pp. 361–371, 2018. doi: 10.5194/angeo-36-361-2018.

[41] S. A. Pulinets, K. A. Boyarchuk, V. V. Hegai, V. P. Kim, and A. M. Lomonosov, "Quasielectrostatic model of atmosphere-thermosphere-ionosphere coupling," *Adv. Space Res.*, vol. 26, no. 8, pp. 1209–1218, 2000. doi: 10.1016/S0273-1177(99)01223-5.

[42] S. A. Pulinets and A. D. Legen'ka, "Spatial–temporal characteristics of large scale disturbances of electron density observed in the ionospheric F-region before strong earthquakes," *Cosmic Res.*, vol. 41, no. 3, pp. 221–230, 2003. doi: 10.1023/A:1024046814173.

[43] S. Pulinets and K. Boyarchuk, *Ionospheric Precursors of Earthquakes*. Berlin, Germany: Springer-Verlag, 2004.

[44] S. Pulinets, "Ionospheric precursors of earthquakes; Recent advances in theoryand practical applications," *Terr. Atmos. Ocean. Sci.*, vol. 15, no. 3, pp. 413–435, 2004. doi: 10.3319/TAO.2004.15.3.413(EP).

[45] S. A. Pulinets, A. N. Kotsarenko, L. Ciraolo, and I. A. Pulinets, "Special case of ionospheric day-to-day variability associated with earthquake preparation," *Adv. Space Res.*, vol. 39, no. 5, pp. 970–977, 2007. doi: 10.1016/j.asr.2006.04.032.

[46] D. Pundhir, B. Singh, S. Op, and S. K. Gupta, "Study of Ionospheric precursors related to an earthquake (M=7.8) of 16 April, 2013 using GPS-TEC measurements: Case study," *Geography Natural Disasters*, vol. 5, no. 1, 2015, Art. no. 1000137. doi: 10.4172/2167-0587.1000137.

[47] P. Sanguansat, *Principal Component Analysis*. Rijeka, Croatia: InTech, 2012, p. 300.

[48] C. J. Schrijver and G. L. Siscoe, *Heliophysics: Space Storms and Radiation: Causes and Effects*. London, U.K.: Cambridge Univ. Press, 2010, p. 472.

[49] G. Sharma, P. K. C. Ray, S. Mohanty, and S. Kannaujiya, "Ionospheric TEC modelling for earthquakes precursors from GNSS data," *Quaternary Int.*, vol. 462, pp. 65–74, Dec. 2017. doi: 10.1016/j.quaint.2017.05.007.

[50] A. F. Sompotan, N. T. Puspito, E. Joelianto, and K. Hattori, "Analysis of ionospheric precursor of earthquake using GIM-TEC, Kriging and neural network," *Asian J. Earth Sci.*, vol. 8, no. 2, pp. 32–44, 2015. doi: 10.3923/ajes.2015.32.44.

[51] P. Tao, X. Feng, and C. Wen, "Image recognition based on two-dimensional principal component analysis combining with wavelet theory and frame theory," *J. Control Sci. Eng.*, vol. 2018, Sep. 2018, Art. no. 9061796. doi: 10.1155/2018/9061796.

[52] M. Ulukavak and M. Yalçinkaya, "Investigation of the relationship between ionospheric TEC anomaly variations and fault types before the earthquakes," *ISPRS Ann. Photogramm., Remote Sens. Spatial Inf. Sci.*, vol. IV-4/W4, pp. 383–388, Oct. 2017. doi: 10.5194/isprs-annals-IV-4-W4-383-2017.
[53] N. Urata, G. Duma, and F. Freund, "Geomagnetic Kp index and earthquakes," *Open J. Earthquake Res.*, vol. 7, no. 1, pp. 39–52, 2018. doi: 10.4236/ojer.2018.71003.
[54] A. N. Vita, S. Y. S. Putra, H. Subakti, and B. Muslim, "Identification of ionospheric GPS TEC anomalies prior to earthquake in Sumatra between 2007-2012 using correlation technique," in *Proc. AIP Conf.*, vol. 1857, no. 1, 2017, Art. no. 040007. doi: 10.1063/1.4987071.
[55] P. Wang, *Solar Physics Research Trends*. Commack, NY, USA: Nova, 2008, p. 411.
[56] Y. Wang, F. Wang, M. Wang, Z.-K. Shen, and Y. Wan, "Coulomb stress change and evolution induced by the 2008 Wenchuan earthquake and its delayed triggering of the 2013 Mw 6.6 Lushan earthquake," *Seismolog. Res. Lett.*, vol. 85, no. 1, pp. 52–59, 2014. doi: 10.1785/0220130111.
[57] X. Wen, H. Zhang, B. Zhou, H. Huang, and Y. Yuan, "Analysis of MODIS satellite thermal infrared information before and after M_S 6.5 Ludian earthquake," in *Geo-Informatics in Resource Management and Sustainable Ecosystem* (Communications in Computer and Information Science), vol. 569. Berlin, Germany: Springer, 2016, pp. 417–433. doi: 10.1007/978-3-662-49155-3_43.
[58] J. Yang, D. D. Zhang, A. F. Frangi, and J. Y. Yang, "Two-dimensional PCA: A new approach to appearance-based face representation and recognition," *IEEE Trans. Pattern Anal. Mach. Intell.*, vol. 26, no. 1, pp. 131–137, 2004. doi: 10.1109/TPAMI.2004.1261097.
[59] P. Zarchan and H. Musoff, *Fundamentals of Kalman Filtering* (Progress in Astronautics and Aeronautics), 3rd ed. Washington, DC, USA: AIAA, 2009, p. 852.
[60] X. Zeng, Y. Lin, W. Chen, Z. Bai, J.-Y. Liu, and C.-H. Chen, "Multiple seismo-anomalies associated with the M6.1 Ludian earthquake on August 3, 2014," *J. Asian Earth Sci.*, vol. 114, pp. 352–361, Dec. 2015. doi: 10.1016/j.jseaes.2015.04.027.
[61] Y. Zhou, J. Yang, F. Zhu, F. Su, L. Hu, and W. Zhai, "Ionospheric disturbances associated with the 2015 M7.8 Nepal earthquake," *Geodesy Geodyn.*, vol. 8, no. 4, pp. 221–228, 2017. doi: 10.1016/j.geog.2017.04.004.
[62] B. Zhao, M. Wang, T. Yu, W. Wan, J. Lei, L. Liu, and B. Ning, "Is an unusual large enhancement of ionospheric electron density linked with the 2008 great Wenchuan earthquake?" *J. Geophys. Res.*, vol. 113, Nov. 2008, Art. no. A11304. doi: 10.1029/2008JA013613.

JYH-WOEI LIN received the B.Sc. degree from the Department of Physics, Chung Yuan Christian University, Chung Li City, Taiwan, in 1989, the M.Sc. degree from the Institute of Geophysics, National Central University, Chung Li City, in 1991, the Ph.D. degree from the Institut für Geophysik, Clausthal-Zellerfeld, Technische Universität Clausthal, Germany, in 2000, and the Ph.D. degree from the Department of Electrical Engineering, Southern Taiwan University of Science and Technology, Tainan, Taiwan, in 2019.

Since 2016, he has been with the Department of Electrical Engineering, Southern Taiwan University of Science and Technology. Until 2019, he has about 61 SCI papers, include artificial intelligence, space physics, geophysics, medical sciences, and remote sensing, especially four books publications in Germany and two books in USA.

JUING-SHIAN CHIOU received the B.S. degree from the Department of Electrical Engineering, Feng Chia University, Taiwan, in 1986, the M.S. degree from the Department of Electrical Engineering, National Central University, Taiwan, in 1990, and the Ph.D. degree from the Department of Electrical Engineering, National Cheng Kung University, Tainan, Taiwan, in 2000.

In 2000, he joined the Department of Electrical Engineering, Southern Taiwan University of Science and Technology, Tainan, Taiwan, where he is currently a Distinguished Professor and a Vice-Dean with the College of Engineering, and also a Vice-President of Taiwan Association for Academic Innovation, and review committee of the Ministry of Science and Technology, Taiwan. He has over 60 articles. His research interests include artificial intelligence, fuzzy control, unmanned aerial vehicles, algorithm, large-scale systems, hybrid systems, and geophysics.

CHUN-TANG CHAO received the B.S. degree from the Department of Electrical Engineering, National Central University, Taiwan, in 1989, the M.S. degree from the Department of Electrical Engineering, National Taiwan University, Taiwan, in 1991, and the Ph.D. degree from the Department of Electrical and Control Engineering, National Chiao Tung University, Hsinchu, Taiwan, in 1995.

In 2000, he joined the Department of Electrical Engineering, Southern Taiwan University of Science and Technology, Tainan, Taiwan, where he is currently an Associate Professor. In 2002, he did a short-term research with the Department of Electrical Engineering, University of Washington, Seattle. His research interests include robotic control, intelligent control systems, artificial intelligence, and geophysics.

Dr. Chao received the Annual Paper Award of the Chinese Engineer Society, in 1993. During his service in Industrial Technology Research Institute of Taiwan, his research on thermal transfer color printer received the gold medal of Outstanding Achievement Award, in 1997.